Nano-particles (NPs) of WO3-type compounds by polyol route with enhanced electrochromic properties

Marie Bourdin, Issam Mjejri, Aline Rougier, Christine Labrugère, Thierry Cardinal, Younès Messaddeq, Manuel Gaudon

▶ **To cite this version:**

Marie Bourdin, Issam Mjejri, Aline Rougier, Christine Labrugère, Thierry Cardinal, et al.. Nano-particles (NPs) of WO3-type compounds by polyol route with enhanced electrochromic properties. Journal of Alloys and Compounds, 2020, 823, 153690 (10 p.). 10.1016/j.jallcom.2020.153690 . hal-02490026

HAL Id: hal-02490026
https://hal.science/hal-02490026v1

Submitted on 5 May 2020

HAL is a multi-disciplinary open access archive for the deposit and dissemination of scientific research documents, whether they are published or not. The documents may come from teaching and research institutions in France or abroad, or from public or private research centers.

L'archive ouverte pluridisciplinaire **HAL**, est destinée au dépôt et à la diffusion de documents scientifiques de niveau recherche, publiés ou non, émanant des établissements d'enseignement et de recherche français ou étrangers, des laboratoires publics ou privés.

Nano-Particles (NPs) of WO_3-type compounds by polyol route with enhanced electrochromic properties.

Marie Bourdin,[†, ∫] *Issam Mjejri,*[†] *Aline Rougier,*[*,†] *Christine Labrugère,*[‡] *Thierry Cardinal,*[†] *Younès Messaddeq,*[∫] *Manuel Gaudon*[*,†]

[†] CNRS, Univ. Bordeaux, Bordeaux INP, ICMCB, UMR 5026, F-33600 Pessac, France

[‡] CNRS, Univ. Bordeaux, PLACAMAT, UMS 3626, F-33600 Pessac, France

[∫] Department of Physics, Center for Optics, Photonics and Lasers (COPL), Laval University, Québec, G1V-0A6, Canada

*Corresponding authors: manuel.gaudon@icmcb.cnrs.fr and aline.rougier@icmcb.cnrs.fr

Abstract

Tungsten trioxide, synthetized as nanoparticles (NPs), then shaped as thin or thick films, has attracted considerable attention as a typical electrochromic material. Herein, the synthesis of WO_3 nanoparticles by the polyol process followed or not by heat-treatments under air or argon, has allowed us to compare the electrochromic activity of powders with different morphologies and oxygen-deficiencies. Only the finest particles associated with pseudo-cubic structure due to a large oxygen-deficiency - on the contrary to the larger particles with standard monoclinic structure and W/O stoichiometric ratio - lead to films showing intense electrochromic color change from a whitish (bleached state) to a dark blue (colored state). Additionally, the as-prepared films exhibit quite fast electrochromic performance and satisfying cycling stability. The sub-stoichiometric nanoparticles prepared from polyol synthesis are of great potential for electrochromic applications.

Keywords. Polyol Synthesis, Nanocrystalline, Tungsten Oxide, Electrochromism

1. Introduction

Tungsten trioxide, as nanoparticles (NPs), thin or thick films, finds many applications in the fields of photocatalysis [1,2], gas sensors [3–6], solar cells [7,8], as well as electrochromism [9–17]. It is generally accepted that the oxidation state of tungsten in WO_3 is mainly +VI, with a corresponding electronic configuration: $6s^0 5d^0$, so the metal center does not have any valence electron. However, its optical and electrical properties are strongly influenced by various defects located in the volume and/or at the surface of the crystals. These defects are directly related to the oxygen vacancies associated with sub-stoichiometric compounds [18]. Hence, considering WO_{3-x} compounds, all along the text, one refers to stoichiometric nanoparticles for $x = 0$, and sub-stoichiometric particles while x is strictly positive. Since the sixties, and the discovery of the electrochromic effect of the WO_3 layers, the technological and scientific interest of this material has grown steadily [19].

Currently, tungsten oxide is the "school-case" electrochromic material, and remains the most widely commercialized. Tungsten trioxide exhibits a range of color that vary from yellow for stoichiometric compounds, to blue for non-stoichiometric ones, due to the reduction of some tungsten cations from W^{6+} to W^{5+} following the creation of oxygen vacancies. Deb [20] discovered the smart coloring properties of WO_3 in thin layers, i.e. the possibility to tune the color of these compounds from an external stimulus, to a blue color shift obtained under UV irradiation (photochromism) or by the application of an electric field (electrochromism). This discovery performed on WO_3 thin layers, aroused great interest for the study of this material shaped as thin films allowing high transparency and then led to the development of electrochromic devices based on WO_3 active layers [10]. In the literature, the deposition of WO_3 films has been reported using various methods, including radio frequency sputtering [18], pulsed laser deposition [13,21], chemical evaporation deposition [22], spray pyrolysis [23] or sol-gel [24]. Obviously, the thickness, the roughness, the density and the crystallite size of the

WO_3 as-prepared films (amorphous state is also largely studied and compared with crystalline layers [25,26]) have a strong impact on their optical properties.

The phenomena involved during electrochromism can be summarized as follows. After deposition in an oxidizing atmosphere allowing the preparation of stoichiometric WO_3 chemical composition, the tungsten oxide films are almost transparent, the bulk color of the solid materials of WO_3 being pale yellow. In electrochromic devices, WO_3 thin films are used as working electrode and placed in contact with an alkaline or protonic electrolyte. Electrochemically induced, a partial reduction of the W^{6+} cation is associated with the insertion of small size ions such as H^+ or Li^+ present in the electrolyte. Whatever the crystalline or amorphous states of the WO_3 compound, as both are associated with corner-sharing octahedral sites with the low-dense ReO_3 structure for crystallized WO_3, the small size ions can be easily inserted in WO_3 bulk. Compensation electrons (to maintain the electroneutrality of the films) need to be co-injected into the oxide network leading to a partial reduction from W^{6+} to W^{5+} ions; therefore a change of color is produced, from colorless WO_3 films (bleached state) to dark blue M_xWO_3 films (colored state). While the M^+ cations are inserted into WO_3, the reversible redox reaction explaining the coloring/bleaching mechanism can be described by the following equation [27]:

$(W^{6+})(O^{2-})_3 + x(M^+) + xe^- \leftrightarrow (M^+)_x(W^{5+}{}_xW^{6+}{}_{1-x})\ (O^{2-})_3$ with $M^+ = H^+$, Li^+, Na^+ or Ag^+.

The bluish coloration is then the consequence of the appearance of an absorption band, due to inter-electronic transfers between the W ions of different oxidation states (intervalence electronic transfer with the equation: $W^{5+} + W^{6+} \rightarrow W^{6+} + W^{5+}$) [28]. The reversibility of the coloring/bleaching mechanism is related to the reversibility of the redox process by insertion/de-insertion according to the direction of polarization of the M^+ ions [27]. Thus, the electrochromic devices allow the fine control of the oxidation states of tungsten ions, that is to

say a control of the electron exchange between the ions W^{5+}, and W^{6+}, [29] and consequently, the fine control of the WO_3 film colors.

In this paper, we propose to study the electrochromic response of three different WO_3 films prepared from different WO_3 powders previously synthetized by the polyol process. For simplicity reason, these three samples are described using the WO_3 formula despite different sub-stoichiometries which are discussed further. The aim is to emphasize the influence of the oxygen sub-stoichiometry in nanometric tungsten oxides on their electrochemical and electrochromic properties. Three different samples with different crystallite sizes, crystalline structures and W/O ratios are compared: the first one is directly obtained from the coprecipitation by polyol route and the two others result from heat treatments performed respectively under air or argon of the raw powder. The electrochemical properties of the films prepared using doctor blading of suspensions made of the three reference powders are measured using a lithiated ionic liquid as electrolyte. Cyclic voltammetry measurements are performed to highlight the electrochemical response in term of amplitude of the as-prepared films. Electrochemical measurements are combined with *ex situ* diffuse reflectance in oxidized and reduced states and *in situ* transmission change of the films at λ = 550 nm and λ = 1000 nm (i.e. in the middle of the visible range and in the near infrared, respectively). Finally, chrono-amperometry measurements illustrate the kinetics of the redox process occurring upon cycling of the films.

2. Experimental

2.1. Synthesis of WO_3 powders

Chemical reagents were purchased from Sigma Aldrich. Tungsten (VI) chloride was used as the soluble tungsten source and diethylene glycol (DEG) as the solvent. WCl_6 (7.2g) was added to 100 mL of DEG and 20 mL of distilled water. The mixture was heated with continuous stirring to 180°C and refluxed for 3 h. At the end of the reaction, a deep blue precipitate was

obtained. The precipitate was washed and centrifuged several times with ethanol to remove the solvent and dried in an oven at 80°C. The powder obtained was then separated into three batches. The as-prepared WO_3 powder constitutes the first batch (raw powder), the powders post-annealed at 600°C under air or under argon being the second and third batches.

2.2. Film preparation

WO_3 films were deposited by the doctor blade technique on glass substrates pre-coated with ITO (In_2O_3:Sn) thin films (SOLEM ITO glass, 30 Ω/□). 500 mg of powder were dispersed in 2 ml of ethanol and stirred for 1 h at room temperature to obtain a homogeneous and viscous suspension. The suspension was then doctor blading on a commercial glass leading to 1 μm thick films.

2.3. Powder and film characterizations

The compound structures were characterized by X-ray diffraction analysis (PANanalytical X'Pert Pro instrument Cu $K_{\alpha 1}$ = 1.54056 Å, $K_{\alpha 2}$ = 1.54439 Å and 2θ range from 8° to 80°).

The morphology of the particles was studied using Transmission electron microscopy (TEM JEOL 2100F microscope) with 120 kV or 200 kV acceleration voltages. Samples were prepared by dispersing a few milligrams of powder in ethanol with ultra-sonication and by direct deposition of one drop of the as-prepared suspension on a carbon grid.

Diffuse absorption spectra were recorded at room temperature from 200 to 1500 nm on a Cary 5000 spectrophotometer using an integration sphere (spectral resolution: 1 nm and band length: 2 nm). Halon was used as white reference. RGB space colorimetric parameters were determined from the spectra using a two-step mathematic treatment. The first step consists in extracting the XYZ tri-stimulus values (defined by the CIE, 1964) from the integration (over the visible range, i.e. from λ = 380 nm up to 780 nm) of the product of x(λ), y(λ) or z(λ) functions (CIE – 1964) with the diffuse reflectance spectra function $X = \int x(\lambda).R(\lambda)d\lambda$. Then, we used the transfer equations defined by the CIE, 1976, to transform the XYZ space to the L*, a* and b* common

three-color space parameters. The spectrophotometer was also used for transmission measurements at λ=550 nm and λ=1000 nm. The spectra are herein presented after Kubelka-Munk transformation. The Kubelka-Munk transformation, where K represents the absorption coefficient and S the diffusion coefficient of the powder, must be only performed while the analysis is made of an opaque powder bed whose grains are distributed randomly and of negligible size compared to the thickness of the analyzed powder bed. So, the relationship between the diffuse reflection (R) and the K/S ratio can be written with the following way equation: $K/S = (1-R)^2/2R$. This K/S ratio accounts for the absorptivity of the powder, the higher the ratio, the greater the absorption.

A ThermoFisher Scientific K-ALPHA spectrometer was used for XPS surface analysis with a monochromatized AlKα source (hν= 1486.6 eV) and a 200 microns X-Ray spot size. A pressure of 10^{-7} Pa was reached in the chamber when transferring the powders pressed onto copper tape. The full spectra (0-1100 eV) were obtained with a constant pass energy of 200 eV and high resolution spectra at a constant pass energy of 40 eV. Charge neutralization was applied during analysis. High resolution spectra (i.e. C1s, O1s, W4f) were quantified and/or fitted using the AVANTAGE software provided by ThermoFisher Scientific (Scofield sensitivity factors used for quantification).

The surface analysis of the films was carried out using the JEOL 6360A scanning electron microscope (SEM) in secondary electron (operating at 5 kV).

The thickness of the films was determined using a WYCO NT1100 optical profilometer.

2.4. Electrochromic measurements

Electrochemical measurements of the WO_3 films on ITO/glass were carried out in a three-electrode cell configuration using a BioLogic SP50 potentiostat/galvanostat apparatus. The operating voltage was controlled between the WO_3 working electrode and saturated calomel electrode, SCE as reference (SCE = 0.234 V/ENH) in between -1.0 and +1.0 V at a scan rate of

20 mV/s, in lithium-based electrolyte (LiTFSI, Solvionic, purity N 99.99%) in 1-etyl-3-methylimidazoliumbis (trifluoromethanesulfonyl)-imide (EMITFSI, purity N 99.99%) using a Pt counter electrode. All the electrochemical measurements were performed at room temperature. The Cary 5000 spectrophotometer previously described was used in transmittance and/or reflectance mode to perform *in situ* or *ex situ* measurements in UV-Vis-NIR range.

3. Results and discussion

3.1. X-ray diffraction, TEM and XPS characterizations of the WO_3 powders

The crystalline structure of the three batches of WO_3 oxide powders was analyzed by X-ray diffraction and the morphology by transmission electron microscopy (**Figure 1**).

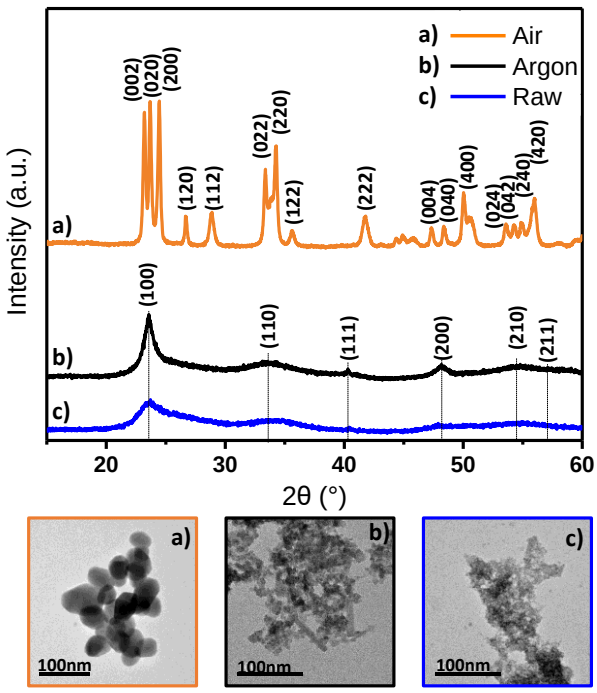

Figure 1. XRD patterns and TEM images of the WO_3 powders synthesized by the polyol process: a) annealed under air, b) annealed under argon, c) raw powder.

The XRD patterns indicate that the raw and argon-annealed powders have similar crystalline structure. The broadening of the diffraction peaks is attributed to the low crystallinity and the small size of the crystallites. Thanks to the most intense diffraction pattern recorded for the argon-annealed powder a pseudo-cubic crystal structure Pm-3m is proposed, whereas the air-

annealed one adopts clearly a $P2_1/n$ monoclinic structure. Whatever the atmosphere of the heat treatment, the as-obtained powders consist of particles of nanometric size: (i) approximatively 5 nm – 10 nm for both the raw powder and the powder annealed under argon and (ii) about 50 nm for the air-annealed powder. In addition, the argon annealed powder appears unstable during the TEM observation forming some nanorods.

The optical properties of the oxide powders (plot of the K/S transformation) are reported in **Figure 2**.

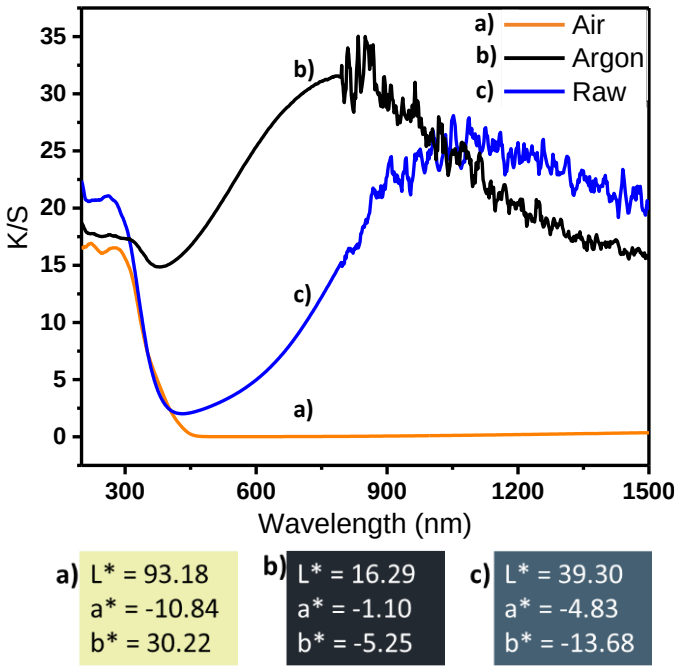

*Figure 2. Diffuse reflectance in K/S and L*a*b* colorimetric parameters associated to their color of the WO_3 powders: a) annealed under air, b) annealed under argon, c) raw powder.*

The reflectance (K/S) spectra show three very different behaviors for the three powders. Firstly, the air annealed powder shows a very strong absorption in the UV and a very low absorption in the visible and the near infrared part of the spectrum, i.e. typical spectrum of a wide-gap semi-conductor. The pale yellowish coloration of this compound (**Figure 2a**) is related to its gap (electronic charge-transfer from valence to conduction band of the semi-conducting oxide), with a gap onset located at about 380 nm, consequently leading to a partial absorption of the

purple hues. The raw-powder (recovered straight after the coprecipitation) shows two strong absorption phenomena: (i) the first one in the UV from the charge transfer and (ii) the second one in the near infra-red at around 1100 nm due to, *a priori*, the intervalence band transfer between W^{5+} and W^{6+} cations. The sample is blue-grey colored (**Figure 2c)**. The argon annealed powder nearly absorbs entirely the whole light wavelengths of the studied range (200 nm – 1500 nm) with a strong absorption band due to the intervalence band transfer centered this time at around 700 nm. It is worth noting that the maximum of the K/S transformation is located at the visible-infrared frontier (700 nm) for the argon-annealed powder whereas it is at 1100 nm in near infrared part for the raw sample. Comparing these two latter samples, the apparent shift of the maximum of absorption could originate from additional absorption centers, which appear in the visible range for the argon annealed sample due to the high density of electron trap centers and the partial filling of the conduction band. It can be also noticed that some authors working on photochromic properties of sub-stoichiometric WO_{3-x} nanoparticles have reported that these oxides after UV irradiation can exhibit a dual absorption bands [30]; hence, the differences between the two samples can be explained as an emphasis of slightly different absorption phenomena that do not occur at the same wavelengths (as, for illustration, an intervalence transfer involving localized or delocalized electrons). Whatever, as consequence, the argon annealed powder exhibits a very dark (nearly black) coloration (**Figure 2b**).

The absorption feature of the raw powder leads to a nearly transparent window in the blue-green range visible spectrum.

The oxidation states of tungsten and oxygen ions in the powders have been studied by XPS analysis. **Figure 3** displays the fitted high resolution XPS spectra of tungsten and oxygen for the three reference powders. Regarding the tungsten ions, the W_{4f} spectra were fitted with some W_{4f5}-W_{4f7} doublets (W^{6+} ions: 37.9 eV and 35.8 eV; W^{5+} ions: 36.3 eV and 34.2 eV). The

air-annealed powder spectrum (**Figure 3a**) shows only W^{6+} ions, whereas both the argon-annealed powder (**Figure 3b**) and the raw powder (**Figure 3c**) show two distinct doublets corresponding to the superimposition of the W^{5+} and the W^{6+} signals [31,32]. The polyol synthesis is carried out in a reducing condition (di-ethylene glycol is a reducing alcohol, used mainly as medium of metallic precipitates [33,34]), the particles obtained at the end of this synthesis are therefore with a chemical composition which is not a stoichiometric WO_3 but having an oxygen sub-stoichiometry leading to the oxide formula: WO_{3-x}. Air annealing clearly produces the full oxidation of the tungsten ions up to the +VI oxidation state. On the opposite, argon annealing is expected to stabilize the W^{5+} ions to the detriment of the W^{6+} ones. Nevertheless, it is worth noting that the W^{5+}/W^{6+} ratio appears a bit smaller than for the raw powder.

The high resolution oxygen spectra (O_{1s} spectra) were fitted with three components. For all the powders, the strongest signal at 530.6 eV corresponds to the oxygen atoms contained in the stoichiometric structure of WO_3 [35]. For powders annealed under argon (**Figure 3b'**) and raw powder (**Figure 3c'**), the signal at 531.9 eV is related to the oxygen atoms derived from sub-stoichiometric WO_{3-x}, i.e. the peak is related to oxygen for which in second neighboring, can be found some anion vacancies. Hence, even for the stoichiometric particles (Figure 3a'), the surface oxygens are in such a situation to neighbor some anionic vacancies, and this characteristic peak still be detected but with low intensity in comparison with the WO_{3-x} sub-stoichiometric compounds. The particles from the raw powder being smaller and the amount of W^{5+} being higher (**Figure 3c**), the amount of oxygen vacancies is greater in this powder than in the one annealed under argon. The signal at 533.1 eV corresponds to oxygens bound to carbon atoms. The presence of carbon in these samples comes from the synthesis route. Indeed, the polyol solvent used is very viscous and it is difficult to completely remove it during washing.

The XPS results clearly confirm the presence of a significant amount of W^{5+} ions on the surface of the WO_3 powders with dark coloration (respectively blue for the raw powder and nearly black for the argon-annealed one). On the other hand, the absence of W^{5+} ions in the air-annealed sample is in good agreement with its pale-yellow color. XPS characterization gives an estimation of the W^{5+} proportion on the powder surfaces. Indeed, it can be assumed that the W^{5+} content occurs with an increasing gradient from the bulk to the surface (the defects, associated with positive local potential, tend to be located near the surface due to their positive energy excess). This effect can lead to an over-estimation of the W^{5+} content form XPS investigations. The estimation of the W^{5+} content in the raw powder is 0.18 and 0.11 in the argon annealed oxides.

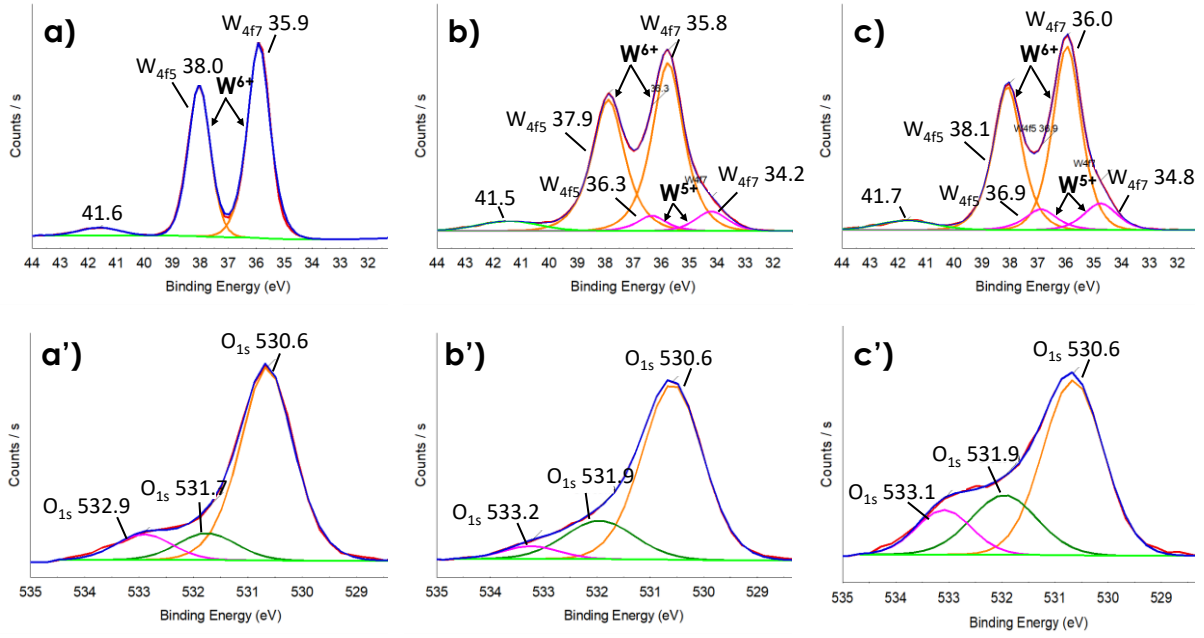

Figure 3. High resolution XPS spectra of W4f (a, b, c) and O1s (a', b', c') in WO_3 powders. a) a') annealed under air, b) b') annealed under argon, c) c') raw powder.

The iodometric titration was also performed in a reproducible way on the blue raw powder (i.e. raw powder) that was easily dissolved in an aqueous solution. Experimentally, the blue powder

was dissolved with a soda pellet and an excess of potassium iodide, and then the I_2 reaction product, formed from the redox process between I^- and W^{5+} ions, was titrated with sodium thiosulfate ($S_2O_4^{2-}$ reducing ion). The tests carried out gave an average delta value of 0.018, so the formula of the raw powder would be $W^{6+}_{0.982}W^{5+}_{0.036}O_{2.982}$ (corresponding to a W^{5+} molar content of 0.036). Hence, it can be concluded from iodometric and XPS measurements that *(i)* the monoclinic powder obtained after annealing treatment is clearly without any traces of W^{5+} (stoichiometric compound); *(ii)* the NPs obtained after argon treatment or after the coprecipitation, both contain a very small amount of W^{5+} ions. XPS has shown higher W^{5+} concentrations determined by extreme surface information only.

3.2. Electrochemical properties of the WO_3 films

The films were doctor bladed from suspensions of the various as-prepared powders in ethanol. The crystallographic structure in between the powders and the films is well maintained as no change was observed using X-ray diffraction. For illustration, despite the broadening, the X-ray pattern of the raw-powder film (**Figure 4a**) shows the occurrence of the pseudo-cubic structure of the WO_3 film, with additional diffraction peaks corresponding to the ITO substrate.

The thickness, and surface morphology: roughness, occurrence of cracks, of the three different films were analyzed by SEM (illustration on the raw-powder film, **Figure 4b**) coupled with optical profilometer measurements (illustration for the raw-powder film, **Figure 4c,d,e,f**). The top-view SEM images of the films show the presence of cracks (with a width of about 1 μm). The roughness coefficient (R_a) of the films is about 1 μm (Ra coefficient is measured as varying between 0.9 and 1 μm depending on the analyzed profile line); the average thickness of the film is difficult to accurately evaluate due to a thickness being of the same order of magnitude than the film roughness. For an approximated but realistic thickness evaluation, one can refer to the profilometer image being taken on a zone of the sample where a part of the substrate is nude, the other one being covered by the film coating. Taking as baseline the height of the substrate

surface, two images, with the same grade of color from blue to red depending on the measured height, were taken, but with different scales : red being associated with height respectively of 1 µm over the substrate surface in the first case (**Figure 4e**) and 1.5 µm in the second case (**Figure 4f**). 50% of the film area is red, so with a height over 1 µm in the first case, whereas significantly less than 50 % of the area is greenish-yellow so below a height of 1.5 µm from the second picture. Hence, the average film thickness can be evaluated in the range 1-1.5 µm.

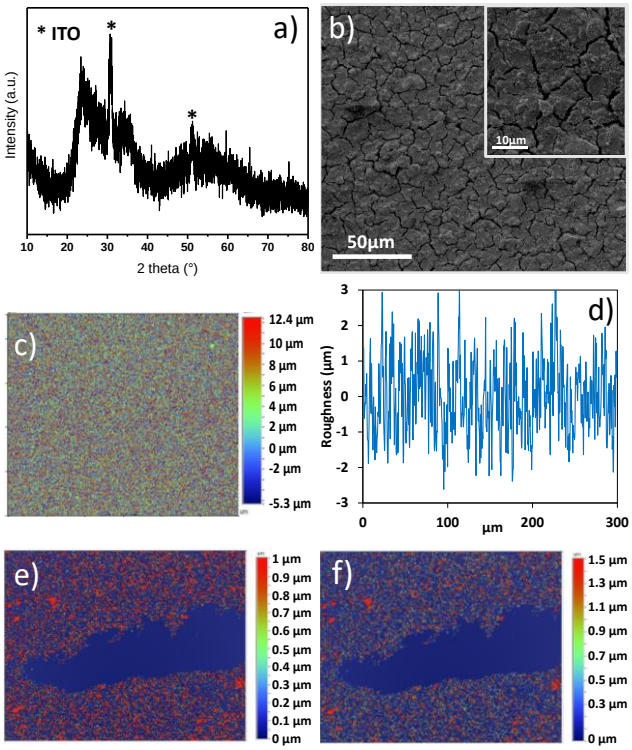

Figure 4. Film doctor bladed from the raw powder (a) XRD pattern, (b) SEM picture (in secondary electron),(c) and (d) 2D-height imaging and line-scan giving the roughness ; (e) and (f) profilometry mapping giving the average film thickness.

Figure 5 shows the cyclic voltammograms for the three films doctor bladed from the raw powder, the powder annealed under argon and the powder annealed under air, cycled in a three-electrode cell, WO_3/LiTFSI in EMITFSI/Pt *vs* SCE. First of all, the CVs of the sub-stoichiometric raw and argon-annealed powders have a significant electrochemical response, whereas the CV shape associated with the powder annealed in air is rather flat underlining a

very limited electrochemical activity. As reported in the literature [29,36], the redox chemical reaction associated with insertion / de-insertion of Li^+ in WO_3 is commonly schematized as follows: $WO_3 + xLi^+ + xe^- \leftrightarrow Li_xWO_3$. The lithium insertion/de-insertion rates (x) can be calculated from the equation: $Q = F.n(WO_3).x$ where Q represents the electrochemical capacity, $F = 96500\ C.mol^{-1}$ and $n(WO_3)$ is the number of moles of the material assuming that the film has an estimated density of 60% considering the method to deposit the films (suspensions obtained from poly-dispersed spherical particles). **Table 1** gathers the Li ions rate of insertion and de-insertion within the tungsten oxide powders.

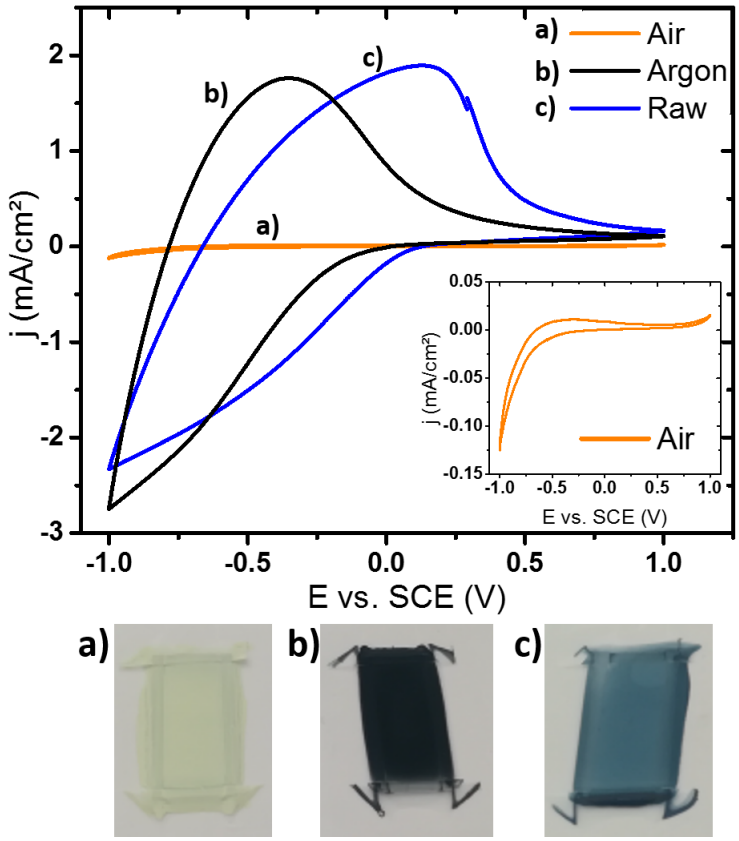

Figure 5. Cyclic voltammograms (fifth cycle) of WO_3/LiTFSI in EMITFSI/Pt vs SCE cells recorded at 20mV/s for films doctor bladed from the three tungsten oxide powders (with corresponding photographs). a) annealed under air, b) annealed under argon, c) raw powder.

Table 1. Li^+ insertion/deinsertion rate (x) for the three tungsten oxide powders.

	Air	Argon	Raw
Li^+ insertion	0.006	0.28	0.33

Li^+ de-insertion	0.002	0.25	0.31

The flat CV shape of the air annealed powder film is associated with a very low x value and no optical activity while the x value being roughly 0.3 for both argon annealed and raw powders suggesting a participation of the third of the W cations in the W^{6+} to W^{5+} reduction process. Hence it is difficult to conclude from this analysis on the participation of bulk ions since, for 5 nm diameter particles more than 30 % of the atoms are located on the surface of the sample.

The switching kinetics of the three samples were deduced from chronoamperometric measurements. The chronoamperograms indicate the current transient (j-t) for potential steps of +1 V /60 s and -1V /60 s. **Figure 6a** only focuses on the second cycle for the three references samples whereas **Figure 6b** gathers two redox cycles but only for the raw powder. Interestingly, both sub-stoichiometric powders showing significant electrochemical activity exhibit oxidation and reduction kinetics with two different behaviors. Indeed, in both cases, the anodic/oxidation peak can be decomposed in three-parts: a first slow decrease (low slope) lasting about 5 seconds followed by another decrease (larger slope) during few more seconds before an asymptotic decrease till the end of the half-cycle. In first approximation, the occurrence of two distinct slopes may be associated with two different de-insertion phenomena; so a trivial assessment would be to assess the first part to a surface de-insertion and the second part to a bulk de-insertion of the lithium ions. On the opposite the cathodic/reduction peak associated with lithium insertion appears regular without any sharp change in term of kinetics.

The film doctor bladed from the air-annealed powder exhibits a single very steep slope, illustrating a fast ions insertion/de-insertion phenomenon. This latter is to be correlated to the negligible electrochemical activity deduced from the CVs that is probably limited to the compound surface. Hence, this trend reinforces the idea that the lithium insertion/deinsertion

kinetics in the first atomic layers of the WO_3 structure is faster than the insertion/deinsertion in deeper crystalline layers.

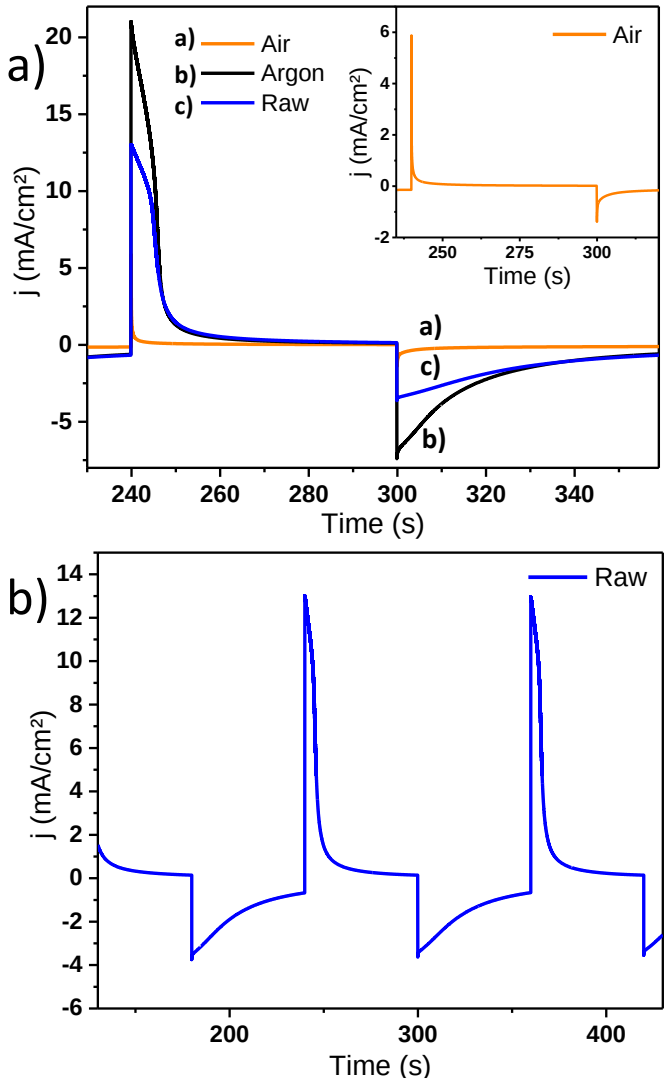

Figure 6. Chronoamperograms of the WO_3 films cycled at -1 V for 60 s and 1 V for 60 s : a) focus on one single cycle for the three samples a) annealed under air, b) annealed under argon, c) raw powder. Inset, CA of the air annealed powder, b) two cycles for the raw powder film.

During the electrochemical measurements, only the film doctor bladed from the raw powder exhibits a significant color change on the contrary to the one annealed in argon despite a similar electrochemical activity. In the literature [37], a significant electrochemical activity was already reported for yellow/monoclinic powder submitted to UV treatment in the film deposition process besides the initial calcination step. The electrochromic response of the raw powder is

associated with a visible color change from dark blue to whitish (**Figure 7a**). Therefore, in the following, the optical properties are restricted to the characterization of the raw powder.

The *in situ* optical properties during the color/bleaching cycling were evaluated by direct transmission measurements at two different wavelengths, namely 550 nm and 1000 nm. The first set of measurements was carried out in the middle of the visible range: at 550 nm, to illustrate the color change of the film, from clear to dark blue (**Figure 7b**). The second measurement was performed in the near infra-red at 1000 nm (**Figure 8**), region on which the optical contrast is supposed to be the greatest because the intervalence band $W^{5+} + W^{6+} \rightarrow W^{6+} + W^{5+}$ is known to be centered at around the micron [25,38].

The measurements show a well reversible behavior with quite good cyclability associated with nice color switch of the film. Nevertheless, the decrease of the transmittance during the coloration process is correlated with a loss of the electrochemical capacity of the film over time. At 550 nm, the whitish state (at +1V) and the blue color (at -1V) are associated with transmittance values of $T_{bleached}$ = 28% and $T_{colored}$ = 5%, the direct optical transmittance modulation is therefore 23%. The low value of the direct transmittance even for the clear state better described for thicker films by the oxidized state of the film, results from large scattering phenomena; indeed, the film is quite thick and not sintered leading to a non-negligible porosity which allows considering that each pore inside the film acts like a scattering center. Nonetheless, the direct transmittance modulation appears rather strong assuming that 60% of the 550 nm light is scattered (i.e. in opaque films, the transmittance characteristics are limited to half of the value, typically on thin films, the bleached state can reach about 85-90% of transmission [21,39]), a further optimization of the elaboration process in order to decrease light scattering can lead to an optical contrast of about 60% prospective optical density (ΔOD) can be roughly estimated to 0.75, using the relation $\Delta OD = \log(T_{bleached}/T_{colored}) = \log(28/5)$. The zoom on one cycle (**Figure 7b**) shows a characteristic peak shape in close relation with the

kinetic aspects commented above from chronoamperometric measurements. Indeed, the peak corresponds to an oxidation process (associated with Li^+ deinsertion) occurring in two distinguished steps: a first sharp increase of the transmission (during around the first 20 s) followed by a slower phenomenon (around 40 s) whereas the decrease of the transmission (reduction process associated with Li^+ insertion) exhibits an asymptotic variation (progressive decrease of the slope) in agreement with the occurrence of only one reduction phenomenon but less and less efficient on the coloration (for a half-cycle equal to 60 s).

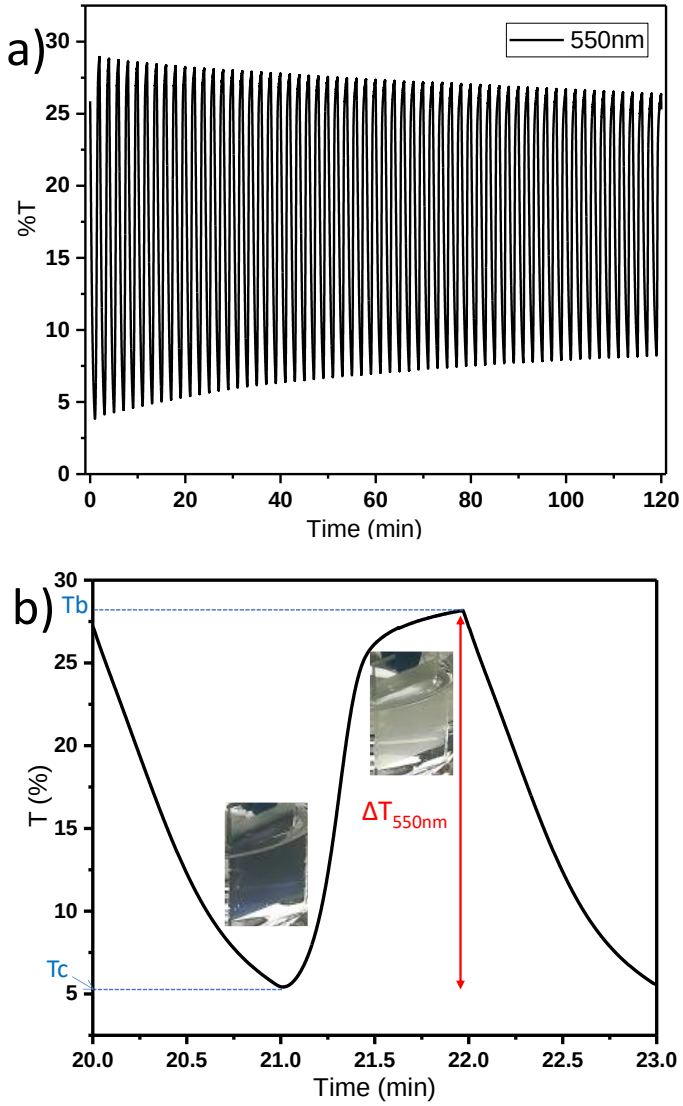

Figure 7. In-situ transmittance curves of the WO_3/LiTFSI in EMITFSI/Pt vs SCE recorded at 550 nm with voltammetry cyclic range from -1 V to +1 V: (a) 60 cycles, (b) focus on one single cycle.

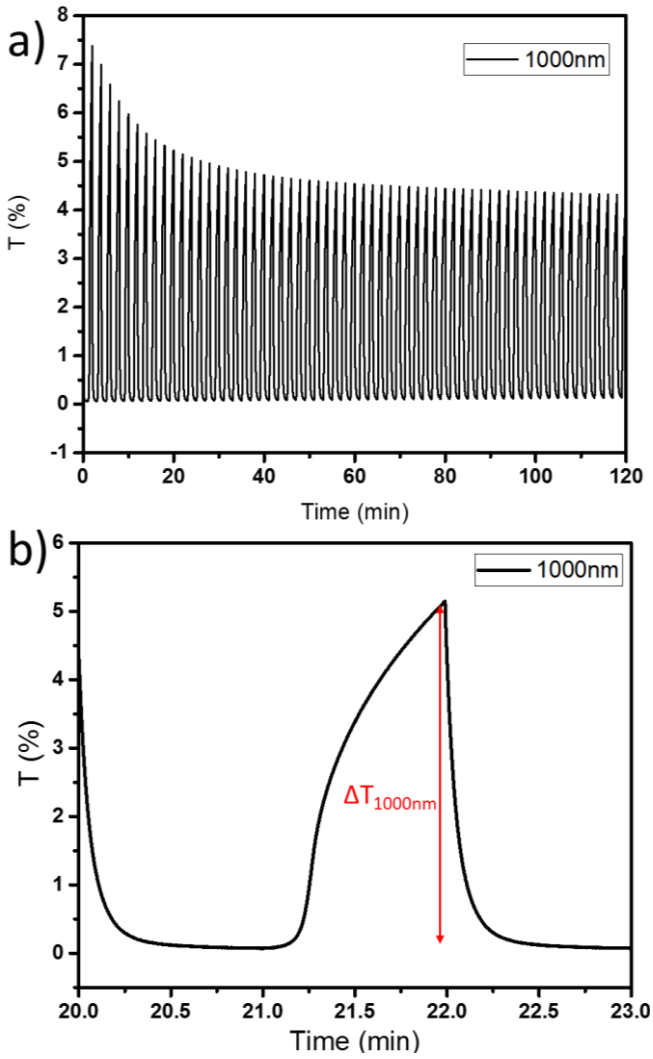

Figure 8. In-situ transmittance curves of the WO_3/LiTFSI in EMITFSI/Pt vs SCE recorded at 1000 nm with voltammetry cyclic range from -1 V to +1 V: (a) 60 cycles, (b) focus on one single cycle. WO_3 films were doctor bladed from the raw powder.

The measurements on the 10 first cycles reported by Deepa et al. on films deposited by dip-coating and spin-coating from WO_3 particles suspensions (i.e. in a work with large similarities with ours) showed response times of a hundred seconds in coloration and about fifty seconds in bleaching [40]. Hence, the as-prepared films, especially the one prepared from the blue WO_{3-x} powder set (i.e. raw powder), exhibit quite fast electrochromic performance.

In the near infra-red, at 1000 nm, the transmittance of the film is nearly zero upon reduction/coloration and of 5% in the oxidized/whitish state (Figure 8). The scattering of the

film, from physical law, possibly changes versus the wavelength but cannot explain such collapse of the transmission efficiency: in a Rayleigh regime, the scattering efficiency decreases versus the wavelength increase and the scattering efficiency is independent of the wavelength in Mie Regime. Actually, a so low transmission for the "oxidized/bleached" state may be due to the color of the raw powder which is pale blue even before the reduction process. That fact is further confirmed from diffuse reflectance measurements performed on oxidized/bleached state film and reduced/colored state film (**Figure 9a**).

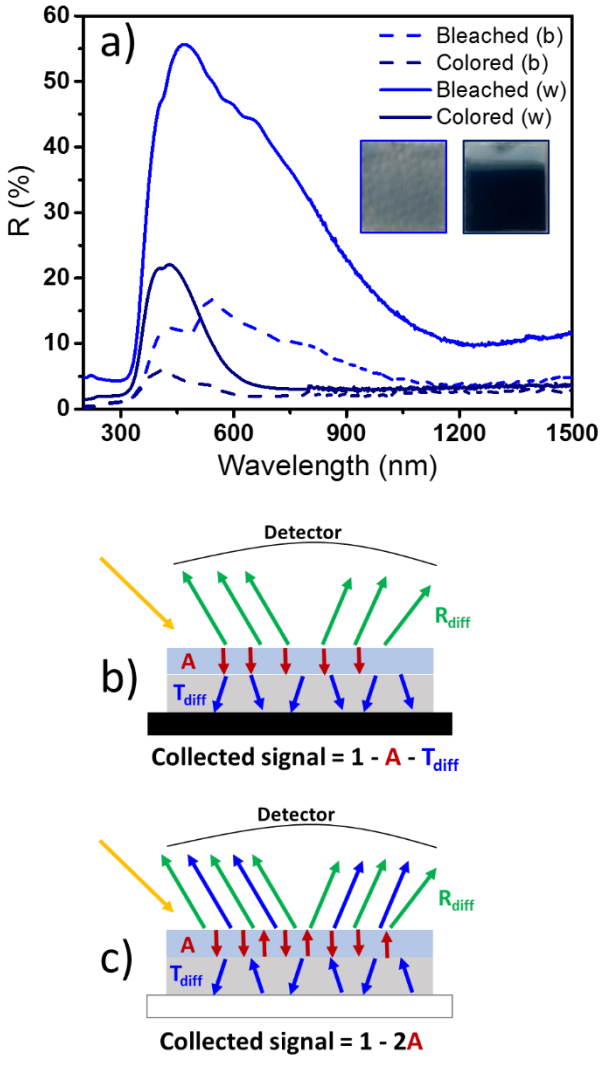

Figure 9. a) Diffuse reflectance on raw film, in the colored and bleached states, made on a black (b) background and white (w) background. Drawing of light passing through the film b) on a black background and c) on a white background.

The kinetic aspect of the signal collected in **Figure 8** exhibits a difference as compared to the signal collected at 550 nm. On **Figure 8a**, the transmittance decreases strongly for the first cycles up to 20 min. The zoom on F**igure 8b** shows a sharp decrease of the transmittance down to 0 in 15 s which tends to be mono-exponential. Such difference between the signal evolution collected at 550 nm and 1000 nm is consistent with the existence of at least two absorbing centers below and above 900 nm as suggested by the diffuse reflectance measurements (**Figure 2**) corresponding respectively to free electrons and W^{5+} centers.

Finally, the diffuse reflectance spectra of films doctor bladed from the raw powder were recorded over the 200 nm - 1500 nm range. The films were studied in reduced/colored and oxidized/bleached states with the ITO/glass substrate placed on a black background (Reflectance: R_{bb}) and on a white background (Reflectance: R_{wb}) as the back side acts as back reflector (**Figures 9b and 9c**). The measurements performed on the black back side make it possible to obtain information on the diffuse reflectance, the collected signal being only the diffuse reflectance of the film (**Figure 9b**). The spectra recorded in the reduced/colored and oxidized/bleached states on a black background are associated with reflectance values of $R_{(bb)}$ = 16.4% and $R_{(cb)}$ = 3.3% at 550 nm corresponding to a modulation reflectance ΔR_{b550} = 13.1%; at 1000 nm the reflectance values are $R_{(bb)}$ = 5.1% and $R_{(cb)}$ = 2.5% with ΔR_{b1000} = 2.6%. The measurements performed on a white back side make it possible to collect both the diffuse reflectance but also the diffuse transmittance of the film, i.e. the complementary part of the electromagnetic light which is not absorbed by the electrochromic film (**Figure 9c**). The recorded spectra are therefore much more intense. The spectra obtained in the reduced/colored and oxidized/bleached states on a white background are associated with reflectance values of $R_{(bw)}$ = 49.4% and $R_{(cw)}$ = 9.2% at 550 nm corresponding to a variation of ΔR_{w550} = 40.2%; in the near infrared, at 1000 nm the reflection values are $R_{(bw)}$ = 16.3% and $R_{(cw)}$ = 3.2% with ΔR_{w1000} = 13.1%. From the shape of the collected signal versus wavelength

from the white back side experiment it appears clearly that even in the oxidized/bleached state a large absorption band centered at roughly 1200 nm corresponding to the intervalence band takes place even for the oxidized/bleached state. The less intense contrast obtained at 1000 nm can be so well explained from the pale blue color of the starting material (sub-stoichiometric WO_{3-x} nanoparticles) that contains before reduction W^{5+} ions in sufficient concentration to produce a significant intervalence absorbing phenomenon.

4. Conclusion

In this study, nanoparticles of WO_3 were synthesized by the polyol process and heat-treated under air and under argon. Structural, morphological and chemical characterizations show that whatever the thermal treatment, the particles are of nanometric sizes; nevertheless larger particles with monoclinic standard structure are obtained after air treatment whereas the raw particles or the ones annealed under argon exhibit a pseudo-cubic structure due to very small crystallite size and/or defects linked to oxygen vacancies. The non-annealed and argon-annealed particles containing W^{6+} and W^{5+} are therefore slightly sub-stoichiometric in oxygen. A 3.6 mol% of tungsten +V was determined using an iodometric titration in the raw powder.

The films shaped by doctor-blade have allowed the investigation of the electrochemical responses to compare the performances between the three as-prepared powders. The voltammetric measurements of films obtained with sub-stoichiometric powders indicate a much higher electrochemical activity and lithium insertion rates than for the stoichiometric film. The raw powder based film shows an interesting electrochromic color change from a whitish (oxidized state / bleached state) to a dark blue (reduced state/ colored state). Moreover, the chronoamperograms coupled with *in situ* transmittance versus cycling indicate that the electrochemical active sub-stoichiometric films exhibit different kinetic behaviors during oxidation and reduction, with an oxidation process occurring in at least three different steps that can be associated with surface and volume lithium ion (de)insertion phenomena. The sub-

stoichiometric nanoparticles prepared from polyol synthesis are, from an electrochemical point of view, of great potential in comparison with the sub-micronic stoichiometric particles.

Acknowledgments

The authors would like to thank Eric Lebraud and Sonia Buffière for their assistance during XRD, SEM & TEM measurements. All authors contributed to the discussions and revisions of the manuscript. The Ph.D. grant of M. Bourdin was supported by the LUMAQ International Associate Laboratory (LIA) between the universities of Laval and Bordeaux.

References

[1] G. Jeevitha, R. Abhinayaa, D. Mangalaraj, N. Ponpandian, Tungsten oxide-graphene oxide (WO_3-GO) nanocomposite as an efficient photocatalyst, antibacterial and anticancer agent, J. Phys. Chem. Solids. 116 (2018) 137–147.
[2] D.P. DePuccio, P. Botella, B. O'Rourke, C.C. Landry, Degradation of Methylene Blue Using Porous WO_3, SiO_2–WO_3, and Their Au-Loaded Analogs: Adsorption and Photocatalytic Studies, ACS Appl. Mater. Interfaces. 7 (2015) 1987–1996.
[3] P.J. Shaver, Activated tungsten oxide gas detectors, Appl. Phys. Lett. 11 (1967) 255–257.
[4] O. Berger, T. Hoffmann, W.-J. Fischer, V. Melev, Tungsten-oxide thin films as novel materials with high sensitivity and selectivity to NO_2, O_3, and H_2S. Part II: Application as gas sensors, J. Mater. Sci. Mater. Electron. 15 (2004) 483–493.
[5] S. Bai, K. Zhang, X. Shu, S. Chen, R. Luo, D. Li, A. Chen, Carboxyl-directed hydrothermal synthesis of WO_3 nanostructures and their morphology-dependent gas-sensing properties, CrystEngComm. 16 (2014) 10210–10217.
[6] A. Boudiba, C. Zhang, C. Navio, C. Bittencourt, R. Snyders, M. Debliquy, Preparation of highly selective, sensitive and stable hydrogen sensors based on Pd-doped tungsten trioxide, Procedia Eng. 5 (2010) 180–183.
[7] H. Simchi, B.E. McCandless, T. Meng, W.N. Shafarman, Structural, optical, and surface properties of WO_3 thin films for solar cells, J. Alloys Compd. 617 (2014) 609–615.
[8] M.M. Rashad, A.E. Shalan, Hydrothermal synthesis of hierarchical WO_3 nanostructures for dye-sensitized solar cells, Appl. Phys. A. 116 (2014) 781–788.
[9] C.G. Granqvist, Electrochromic tungsten oxide films: Review of progress 1993–1998, Sol. Energy Mater. Sol. Cells. 60 (2000) 201–262.
[10] C.G. Granqvist, Electrochromics for smart windows: Oxide-based thin films and devices, Thin Solid Films. 564 (2014) 1–38.
[11] M. Deepa, A.K. Srivastava, S. Lauterbach, Govind, S.M. Shivaprasad, K.N. Sood, Electro-optical response of tungsten oxide thin film nanostructures processed by a template-assisted electrodeposition route, Acta Mater. 55 (2007) 6095–6107.
[12] M. Rakibuddin, H. Kim, Synthesis and characterization of facile industrially scalable and cost effective WO_3 micro–nanostructures for electrochromic devices and photocatalyst, Ceram. Int. 44 (2018) 16615–16623. doi:10.1016/j.ceramint.2018.06.088.
[13] A. Rougier, F. Portemer, A. Quédé, M. El Marssi, Characterization of pulsed laser deposited WO_3 thin films for electrochromic devices, Appl. Surf. Sci. 153 (1999) 1–9.

[14] K. Sauvet, A. Rougier, L. Sauques, Electrochromic WO_3 thin films active in the IR region, Sol. Energy Mater. Sol. Cells. 92 (2008) 209–215.
[15] K. Sauvet, L. Sauques, A. Rougier, IR electrochromic WO_3 thin films: From optimization to devices, Sol. Energy Mater. Sol. Cells. 93 (2009) 2045–2049.
[16] D. Ma, T. Li, Z. Xu, L. Wang, J. Wang, Electrochromic devices based on tungsten oxide films with honeycomb-like nanostructures and nanoribbons array, Sol. Energy Mater. Sol. Cells. 177 (2019) pp. 51-56.
[17] A; Maho, S. Nicolay, L. Manceriu, L., G. Spronck, C; Henrista, R. Clootsa, B. Vertruyen, P. Colson, Comparison of indium tin oxide and indium tungsten oxide as transparent conductive substrates for WO_3-based electrochromic devices, J. Electrochem. Soc. 164 (2017) H25-H31.
[18] A.M. Stoneham, Ceramic Surfaces: Theoretical Studies, J. Am. Ceram. Soc. 64 (1981) 54–60.
[19] S.K. Deb, A Novel Electrophotographic System, Appl. Opt. 8 (1969) 192–195.
[20] K. Sauvet, L. Sauques, A. Rougier, Electrochromic properties of WO_3 as a single layer and in a full device: From the visible to the infrared, J. Phys. Chem. Solids. 71 (2010) 696–699.
[21] Y.S. Zou, Y.C. Zhang, D. Lou, H.P. Wang, L. Gu, Y.H. Dong, K. Dou, X.F. Song, H.B. Zeng, Structural and optical properties of WO_3 films deposited by pulsed laser deposition, J. Alloys Compd. 583 (2014) 465–470.
[22] C.S. Blackman, I.P. Parkin, Atmospheric Pressure Chemical Vapor Deposition of Crystalline Monoclinic WO_3 and WO_{3-x} Thin Films from Reaction of WCl_6 with O-Containing Solvents and Their Photochromic and Electrochromic Properties, Chem. Mater. 17 (2005) 1583–1590.
[23] D.R. Acosta, C. Magaña, F. Hernández, J. Ortega, Electrical, optical and electrochromic properties of Ti:WO_3 thin films deposited by the pulsed chemical spray technique, Thin Solid Films. 594 (2015) 207–214.
[24] N. Özer, Optical and electrochemical characteristics of sol-gel deposited tungsten oxide films: a comparison, Thin Solid Films. 304 (1997) 310–314.
[25] O.F. Schirmer, V. Wittwer, G. Baur, G. Brandt, Dependence of WO_3 Electrochromic Absorption on Crystallinity, J. Electrochem. Soc. 124 (1977) 749–753.
[26] S.-H. Lee, H.M. Cheong, C.E. Tracy, A. Mascarenhas, A.W. Czanderna, S.K. Deb, Electrochromic coloration efficiency of a-WO_{3-y} thin films as a function of oxygen deficiency, Appl. Phys. Lett. 75 (1999) 1541–1543.
[27] B.W. Faughnan, R.S. Crandall, Electrochromic displays based on WO_3, in: J.I. Pankove (Ed.), Disp. Devices, Springer Berlin Heidelberg, Berlin, Heidelberg, 1980: pp. 181–211.
[28] B.W. Faughnan, R.S. Crandall, P.M. Heyman, Electrochromism in WO_3 Amorphous Films, RCA Rev. 36 (1975) 177–197.
[29] G.A. Niklasson, C.G. Granqvist, Electrochromics for smart windows: thin films of tungsten oxide and nickel oxide, and devices based on these, J. Mater. Chem. 17 (2006)
[30] Q. Liu, C. Hu, X. Wang, Hydrothermal synthesis of oxygen-deficiency tungsten oxide quantum dots with excellent photochromic reversibility, App. Surf. Sc. 480 (2019) 404-409
[31] T.H. Fleisch, G.J. Mains, An XPS study of the UV reduction and photochromism of MoO_3 and WO_3, J. Chem. Phys. 76 (1982) 780–786.
[32] J. Diaz-Reyes, R. Castillo-Ojeda, M. Galvan-Arellano, O. Zaca-Moran, Characterization of WO_3 Thin Films Grown on Silicon by HFMOD, Adv. Condens. Matter Phys. (2013).
[33] F. Fievet, J.P. Lagier, B. Blin, B. Beaudoin, M. Figlarz, Homogeneous and heterogeneous nucleations in the polyol process for the preparation of micron and submicron size metal particles, Solid State Ion. 32–33 (1989) 198–205.

[34] H. Dong, Y.-C. Chen, C. Feldmann, Polyol synthesis of nanoparticles: status and options regarding metals, oxides, chalcogenides, and non-metal elements, Green Chem. 17 (2015) 4107–4132.
[35] H.Y. Wong, C.W. Ong, R.W.M. Kwok, K.W. Wong, S.P. Wong, W.Y. Cheung, Effects of ion beam bombardment on electrochromic tungsten oxide films studied by X-ray photoelectron spectroscopy and Rutherford back-scattering, Thin Solid Films. 376 (2000) 131–139.
[36] C.G. Granqvist, Handbook of Inorganic Electrochromic Materials, Elsevier, 1995.
[37] A. Danine, L. Cojocaru, C. Faure, C. Olivier, T. Toupance, G. Campet, A. Rougier, Room Temperature UV treated WO_3 thin films for electrochromic devices on paper substrate, Electrochimica Acta. 129 (2014) 113–119.
[38] Y. Shigesato, Photochromic Properties of Amorphous WO_3 Films, Jpn. J. Appl. Phys. 30 (1991) 1457.
[39] M. Deepa, A.K. Srivastava, S.A. Agnihotry, Influence of annealing on electrochromic performance of template assisted, electrochemically grown, nanostructured assembly of tungsten oxide, Acta Mater. 54 (2006) 4583–4595.
[40] M. Deepa, T.K. Saxena, D.P. Singh, K. N. Sood, S.A. Agnihotry, Spin coated versus dip coated electrochromic tungsten oxide films: Structure, morphology, optical and electrochemical properties, Electrochimica Acta. 51 (2006) 1974-1989.